In-beam γ-ray spectroscopy of ^{35}Mg via knockout reactions at intermediate energies

S. Momiyama,[1,*] P. Doornenbal,[2] H. Scheit,[2,3] S. Takeuchi,[2,†] M. Niikura,[1] N. Aoi,[2,‡] K. Li,[2,4] M. Matsushita,[2,5] D. Steppenbeck,[2] H. Wang,[2,4] H. Baba,[2] E. Ideguchi,[6,§] M. Kimura,[7] N. Kobayashi,[8,‖] Y. Kondo,[8] J. Lee,[2,¶] S. Michimasa,[6] T. Motobayashi,[2] N. Shimizu,[6] M. Takechi,[2,**] Y. Togano,[2,††] Y. Utsuno,[9] K. Yoneda,[2] and H. Sakurai[1,2]

[1]*Department of Physics, University of Tokyo, Bunkyo, Tokyo 113-0033, Japan*
[2]*RIKEN Nishina Center, Wako, Saitama 351-0198, Japan*
[3]*Institut für Kernphysik, Technische Universität Darmstadt, 64289 Darmstadt, Germany*
[4]*Peking University, Beijing 100871, China*
[5]*Department of Physics, Rikkyo University, Toshima, Tokyo 172-8501, Japan*
[6]*Center for Nuclear Study, University of Tokyo, RIKEN Campus, Wako, Saitama 351-0198, Japan*
[7]*Department of Physics, Hokkaido University, Sapporo 001-0021, Japan*
[8]*Department of Physics, Tokyo Institute of Technology, Meguro, Tokyo 152-8551, Japan*
[9]*Japan Atomic Energy Agency, Tokai, Ibaraki 319-1195, Japan*

(Received 14 April 2017; published 29 September 2017)

The isotope ^{35}Mg was spectroscopically studied via nucleon-removal reactions from ^{36}Mg and ^{37}Al secondary beams at intermediate energies. The experiment's aim was to clarify the level structure of this nucleus located in between the $N = 20$ and 28 shell quenchings. De-excitation γ-ray energies, exclusive cross sections, and parallel momentum of outgoing ^{35}Mg for several final states were measured and compared to structure calculations in the shell model and antisymmetrized molecular dynamics framework and the eikonal reaction calculation, further developing the level scheme of ^{35}Mg. It was found that a large fraction of the one-neutron knockout reaction goes into unbound states of ^{35}Mg, which may explain missing f-wave strength.

DOI: 10.1103/PhysRevC.96.034328

I. INTRODUCTION

Atomic nuclei with proton numbers in the range $Z =$ 10–12 and neutron numbers in the range $N =$ 20–22, a region termed the "island of inversion" [1], are known to possess unusual masses, low 2^+_1 excitation energies, and large collectivities in spite of their proximity to the neutron magic number $N = 20$ [1–9]. This phenomenon is well explained by neutron intruder configurations ($2p$-$2h$ [$\nu(sd)^{-2}(fp)^{+2}$]) across a reduced $N = 20$ gap already in the ground state [1,10] and was confirmed experimentally by one-neutron knockout reactions [11]. Besides $N = 20$, another magic number well established around the line of β stability and disappearing for neutron-rich nuclei is found at $N = 28$. Here, the large energy gap originates from the $\nu f_{5/2}$-$\nu f_{7/2}$ spin-orbit splitting. Recent findings of a low 2^+_1 excitation energy for ^{42}Si revealed the vanishing of the $N = 28$ magic number [12,13]. In fact, a reduction of the shell gap was observed already for ^{46}Ar [14], which is only two protons away from the stable doubly magic nucleus ^{48}Ca.

Originally, these two regions were conceived as separate areas of the Segré chart, with clear edges of the island of inversion [1]. However, later research showed that also for ^{36}Mg the ground state is dominated by neutron $2p$-$2h$ configurations [15,16]. Further investigations of this nucleus revealed a large deformation length and $B(E2)\uparrow$ from inelastic scattering on liquid hydrogen, carbon, and lead targets [17,18], and the $E(4^+_1)/E(2^+_1)$ remains high up to the $N = 26$ isotope ^{38}Mg [19]. These experimental results suggest that the two shell-quenching regions at $N = 20$ and 28 merge and form a big island of deformation [20]. In order to further elucidate the driving mechanisms of shell evolution in this area, it is necessary to figure out the location of the neutron single-particle orbits.

A powerful tool to study these orbits is one-neutron knockout reactions. The cross section of each final state can be related to the occupancy of neutrons in an orbit by means of theoretical calculations based on eikonal and sudden approximations [21,22]. Furthermore, the parallel momentum distributions of the reaction residues reflect the orbital angular momentum (l value) of the knocked-out neutron [21,23–25], allowing for the assignment of spin parity of the individual final state. Combining the experimental values and theoretical reaction calculations based on the eikonal theory allows for the deduction of the spectroscopic information of such neutron-rich nuclei. In addition, comparisons to other reaction channels and observed intensities may help to reveal whether observed γ rays originate from the same or different levels. In a previous

*momiyama@nucl.phys.s.u-tokyo.ac.jp
†Present address: Department of Physics, Tokyo Institute of Technology, Meguro, Tokyo 152-8551, Japan.
‡Present address: Research Center for Nuclear Physics, Osaka University, Ibaraki, Osaka 567-0047, Japan.
§Present address: Research Center for Nuclear Physics, Osaka University, Ibaraki, Osaka 567-0047, Japan.
‖Present address: Research Center for Nuclear Physics, Osaka University, Ibaraki, Osaka 567-0047, Japan.
¶Present address: Department of Physics, University of Hong Kong, Pokfulam Road, Hong Kong.
**Present address: Graduate School of Science and Technology, Niigata University, Niigata 950-2102, Japan.
††Present address: Department of Physics, Tokyo Institute of Technology, Meguro, Tokyo 152-8551, Japan.

experiment, three γ-ray transitions of decaying excited states in ^{35}Mg were reported following nucleon removal from a ^{38}Si secondary beam [26]. In this context, results of the one-neutron knockout reaction from ^{36}Mg and the two-nucleon removal reaction from ^{37}Al on a carbon target at intermediate energies around 200 MeV/nucleon are reported.

II. EXPERIMENT

The experiment was carried out at the Radioactive Isotope Beam Factory, operated by the RIKEN Nishina Center and the Center for Nuclear Study of the University of Tokyo. A primary beam of ^{48}Ca with an average intensity of 70 particle nA and an energy of 345 MeV/nucleon was directed on a 15-mm-thick rotating Be target located at the BigRIPS radioactive isotope projectile-fragment separator's entrance [27]. From the multitude of reaction products, secondary beams composed mainly of ^{37}Al and ^{36}Mg were selected and purified via the $B\rho$-ΔE-$B\rho$ method, and identified with the ΔE-$B\rho$-TOF method [28], for which the time of flight (TOF), magnetic rigidity ($B\rho$), and energy loss (ΔE) are used to determine the mass-to-charge ratio (A/Q) and element number (Z). The $B\rho$ values of BigRIPS were optimized for ^{36}Mg and the momentum acceptance ($\Delta P/P$) was set to $\pm 3\%$. The ΔE was measured by an ionization chamber at F7 [29], the $B\rho$ was determined from the position information measured by parallel-plate avalanche counters (PPAC) [30] at F5 and F7, and the TOF was recorded between two plastic scintillators placed at F5 and F7. The rate of ^{36}Mg and ^{37}Al isotopes transported through BigRIPS were 80 and 350 particles/s, respectively.

The secondary beams were incident on a 2.54 g/cm^2 thick carbon reaction target. The average energies for ^{36}Mg and ^{37}Al isotopes was 235 and 246 MeV/nucleon in front of the reaction target. Reaction residues produced from the secondary beams were selected and identified by the Zero Degree spectrometer (ZDS) [27]. $B\rho$ values in ZDS were tuned to the one-neutron knockout channel from ^{36}Mg to ^{35}Mg. The TOF values were measured by two plastic scintillators located at F8 and F11, the ΔE was measured by an ionization chamber placed at F11, and the $B\rho$ was deduced by the position measurement using PPACs at F8 and F9. The resulting particle-identification spectrum for ZDS is shown in Fig. 1 for ^{36}Mg ions identified in BigRIPS.

To detect γ rays emitted from excited states of ^{35}Mg, the reaction target was surrounded by the high-efficiency γ-ray detector array DALI2 [31,32], which consisted of 186 large-volume NaI(Tl) crystals positioned at angles of $\sim$20–150° relative to the beam axis. The energy resolution and the efficiency were 10% (FWHM) and 20% for 1-MeV γ rays, respectively. Applying add-back, for which all energy depositions were summed for crystals with centers within 15 cm from the crystal with the highest energy deposition, increased the efficiency to 26%. The array was calibrated using standard ^{60}Co, ^{88}Y, and ^{137}Cs radiation sources and the determination of the efficiency agreed within 6% to simulations using the GEANT4 framework [33].

The parallel momentum distribution ($P_{//}$) of ^{35}Mg following one-neutron knockout reactions was also measured in this study. The momentum of a reaction residue in the projectile rest frame was deduced by the Lorentz transformation of the laboratory frame momentum obtained using the TOF values between F8 and F11, which was corrected by the projectile velocity deduced by the TOF between F3 and F7. Data were accumulated for approximately 10 h.

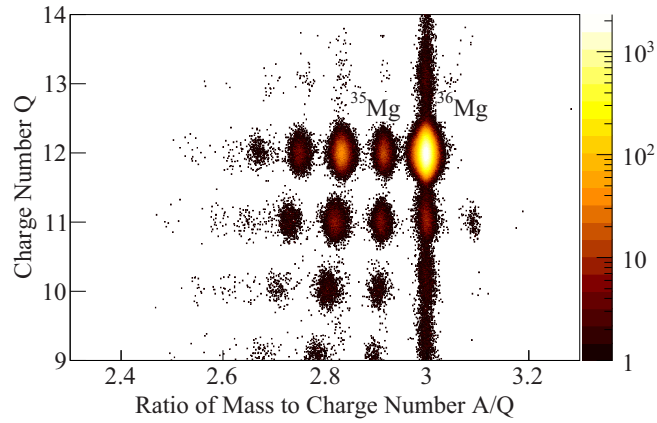

FIG. 1. Particle-identification plot of reaction residues detected in the Zero Degree spectrometer. A gate was imposed on the ^{36}Mg ions passing the BigRIPS spectrometer.

III. ANALYSIS AND EXPERIMENTAL RESULTS

Figure 2 shows the obtained γ-ray spectra for ^{35}Mg after applying the Doppler correction for detectors with azimuthal angles $\vartheta \leqslant 65°$. The angular range was selected to suppress low-energy contributions from the atomic background, enabling the observation of γ-ray transitions above $\sim$200 keV, as demonstrated in the spectroscopy of ^{29}Ne [34]. The Doppler shift was corrected with the midtarget velocity of the reaction residue calculated by the ATIMA code [35]. The γ-ray energies were determined by fit of response functions obtained from simulations using the GEANT4 framework [33]. In these simulations, the NaI(Tl) crystal housings and the Al beam pipe were taken into account in order to reproduce the response function of the DALI2 array. Systematic errors of the γ-ray energy and efficiency were deduced to be 4 keV and 6% in comparison with the experimental data of standard radiation sources placed at the secondary target position. The experimental spectra were fitted with the resulting DALI2 response functions using the intensities and two exponentials for the background as free parameters. The fitting results are also displayed in Fig. 2.

Three γ-ray transitions emitted from ^{35}Mg were already observed in the previous two-step fragmentation experiment from a ^{38}Si secondary beam and their energies were reported as 446(5), 621(7), and 670(8) keV [26]. In that experiment, similar intensities were observed for the latter two transitions. In the present work, a candidate for a new transition was observed at 206(8) keV, while deduced γ-ray energies for the two known transitions were 443(7) and 616(8) keV. For the combined spectra of $1n$-knockout and $1p1n$-removal reactions, the confidence level of the 206(8)-keV transition is 3.1 σ. Due to the resolution of DALI2, the transition reported at 670(8) keV by Ref. [26] would overlap with the one observed

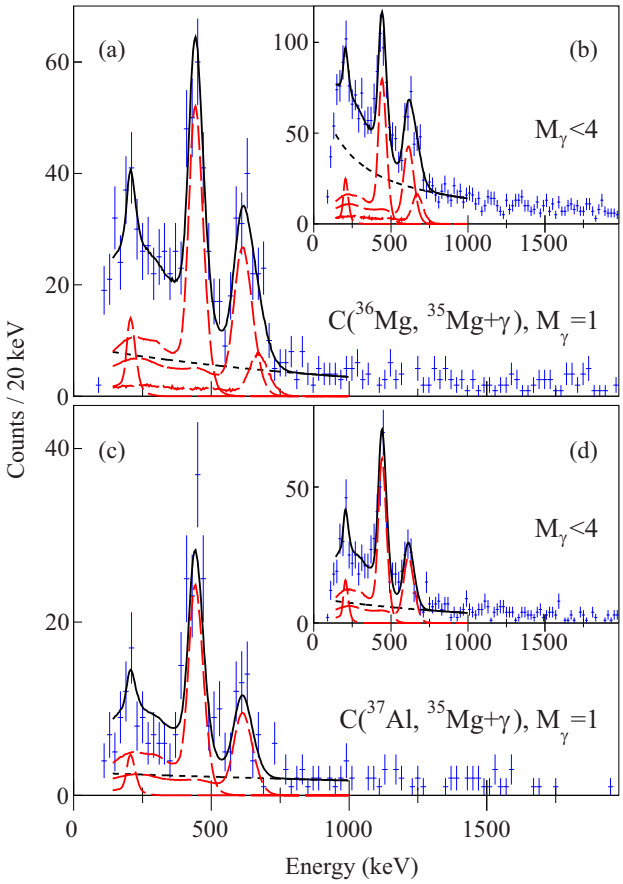

FIG. 2. Doppler corrected γ-ray energy spectra in coincidence with ^{35}Mg fragments following one-neutron knockout reactions (top) and two-nucleon removal from ^{37}Al (bottom). For panels (a) and (c), data were analyzed only for events with a γ-ray multiplicity of one ($M_\gamma = 1$). The insets (b) and (d) show the spectra with a condition of $M_\gamma < 4$. Red long dashed lines represent the simulated response functions at the respective observed γ-ray energies. The black short dashed lines correspond to the fitted background, while the overlaid black solid curves are the result of the statistical fits.

at 616(8) keV in the present work. It was included into the fits of the observed spectra. Small contributions were only found for the one-neutron knockout, while the spectrum for the nucleon removal from ^{37}Al can be described without this transition. This difference of the γ-ray emission between two reaction channels suggests that the 616(8)- and 670(8)-keV γ rays were emitted from two different excited states. It is also noted that Ref. [26] did not observe the 206(8)-keV transition, indicating that it originates from a new level that was not or only weakly populated in that reaction. For the energy determination, besides the errors of fitting and the energy calibration mentioned above, the systematic error caused by the unknown lifetime of excited states was considered, as described, e.g., in Ref. [9,36]. No clear γ-γ coincidence was observed. Furthermore, the one-neutron separation energy of ^{35}Mg was deduced to be 750(180) keV by mass measurements [37]. This low separation energy and observation of no cascade decay support the assumption that all the observed γ rays were emitted independently and either decay into the ground state or a low-lying level below the detection threshold of about 200 keV. The experimentally suggested level scheme of ^{35}Mg is shown in Fig. 4.

TABLE I. Experimental inclusive and γ-ray emission cross sections.

Reaction	E_γ (MeV)	σ (mb)
C(^{36}Mg, ^{35}Mg)		37(3)
	206(8)	2(1)
	443(7)	8(1)
	616(8)	7(1)
	670(8)	3(1)
C(^{36}Mg, ^{34}Mg)		135(12)
C(^{36}Mg, ^{33}Mg)		64(13)

To determine both the inclusive and exclusive cross sections for the one-neutron knockout reaction from ^{36}Mg, it was necessary to deduce the transmission of ^{35}Mg through ZDS to correct for the reaction losses in the thick secondary target and the acceptance of ZDS. For this purpose, ZDS was centered to ^{36}Mg and the transmission for this nucleus was deduced to 75(3)%. This value was used for the transmission estimation of the one-neutron knockout channel. Further, two plastic scintillators with a total thickness of 3 mm were placed in front of the secondary target. The reaction rate in these two scintillators was estimated by LISE++ calculations [38] and subtracted from the experimental inclusive cross section. As a result, the inclusive one-neutron knockout cross section from ^{36}Mg was determined to be 37(3) mb, while γ-ray emission cross sections were deduced to 2(1), 8(1), 7(1), and 3(1) mb for the 206(8)-, 443(7)-, 616(8)-, and the 670(8)-keV transitions, respectively, as summarized in Table I. Note that the cross sections for populating the 443(7)- and 616(8)-keV transitions were deduced using all γ-ray detectors without any restriction on the γ-ray multiplicity. Since 206(8)- and 670(8)-keV peaks were hardly visible and it was difficult to deduce their cross sections under this condition, they were estimated by intensity comparison relative to the 616(8)-keV transition under low M_γ conditions using only forward-angle γ-ray detectors. The quoted cross-sectional errors consist of contributions from the statistical errors of both ^{36}Mg and ^{35}Mg passing BigRIPS and ZDS, the efficiency error of PID detectors, and the error in the transmission analysis, as well as the γ-ray angular distribution, all added in quadrature. An error of 7% was assumed for the angular distribution, based on the different efficiencies between a calculated 50% prolate alignment using the framework of the reaction calculation described below and an isotropic distribution [39]. The uncertainty in the detector efficiency for PID and transmission was estimated by independent deduction of these values in every run and taking the root-mean-square deviation. In addition, the two-neutron and three-neutron removal cross sections were determined to be 135(12) and 64(13) mb, respectively, much larger than for the one-neutron knockout. They are also shown in Table I.

Figure 3(a) shows the measured inclusive parallel momentum distribution of ^{35}Mg following the one-neutron knockout

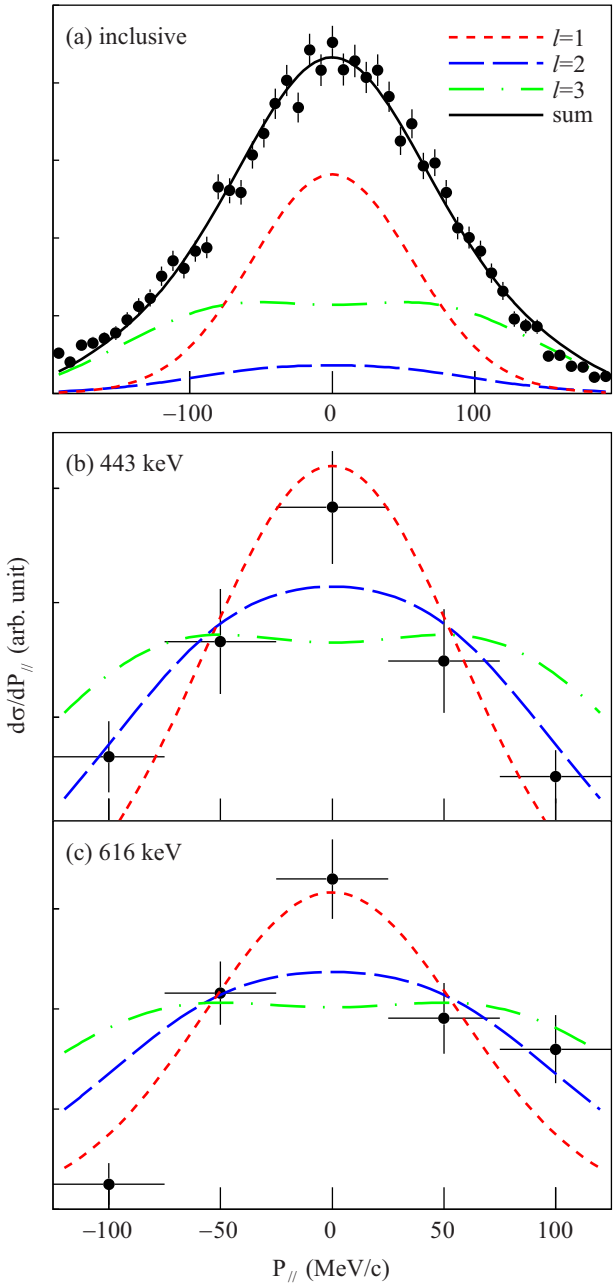

FIG. 3. Measured parallel momentum distribution of ^{35}Mg following the 1n-knockout reaction (a) in the inclusive channel, (b) coincident with the 443(7)-keV γ ray, and (c) coincident with the 616(8)-keV γ ray. Red, blue, and green lines show the theoretical parallel momenta with $l = 1$, 2, and 3 orbits, respectively. The black line in panel (a) corresponds to the sum of the fit containing these three lines. In panels (b) and (c) each theoretical line is normalized by the total counts of experimental data.

reactions in the rest frame of ^{36}Mg. The experimental data are fitted by calculations of the eikonal reaction theory using the CSC_GM code [25]. It was assumed that the excitation energy equals zero for the inclusive momentum distribution. The calculations were convoluted by the intrinsic parallel momentum resolution of the experimental setup. This parallel momentum resolution had two components: First, the energy straggling caused by the reaction target and the detector resolution, and second, the energy loss difference in the reaction target between the ^{36}Mg secondary beam and the ^{35}Mg reaction residues. The former was measured using the ^{36}Mg secondary beam on the reaction target and through ZDS, resulting in 28 MeV/c. The latter was calculated with the ATIMA code [35] to be 14 MeV/c, resulting in a resolution of 31 MeV/c. The fitting result of the inclusive momentum distribution is displayed in Fig. 3(a) as the black curve. It is well explained by a neutron knocked out to 48(1)% from $l = 1$ and to 42(1)% from $l = 3$ orbits, while $l = 2$ components are small at 10(1)%. It is worth noting that there are significant components of neutron knockout from not only the $l = 3$ but also the $l = 1$ orbit, though ^{36}Mg has only 24 neutrons.

Similarly, Fig. 3(b) and 3(c) show exclusive momentum distributions in coincidence with the 443(7)- and 616(8)-keV transitions, respectively, while statistics were insufficient for 206(8)- and 670(8)-keV transitions. These distributions were obtained by fitting the γ-ray energy spectra for every 50-MeV/c $P_{//}$ bin and getting the respective intensities. Theoretical distributions were normalized by corresponding γ-ray counts in these figures. Reduced χ^2 values of $P_{//}$ for the 443(7)-keV [616(8)-keV] transitions compared with theoretical distributions of knockout from $l = 1$ and 2 orbits are 4.01 and 1.36 (7.47 and 9.82), respectively. This result implies that the excited state emitting the 443(7)-keV [616(8)-keV] γ ray was produced by one-neutron knockout from the d (p) orbit. However, these χ^2 values are too ambiguous to distinguish momentum distributions of one-neutron knockout from p and d orbits because of the limited statistics. On the other hand, the possibility of one-neutron knockout from the $l = 3$ orbit is clearly excluded. Combining the analysis of inclusive and exclusive momentum distributions, excited states populated by neutron knockout from the $l = 3$ orbit may lie in the low-energy region or emit multiple low-energy γ rays which were difficult for this experimental setup to observe.

IV. DISCUSSION

The experimental data were confronted with two different theoretical approaches. First, shell-model calculations with two kinds of interactions and model spaces were performed using the KSHELL code [40]. One of the selected interactions was the SDPF-M interaction [41] with a model space including the sd shell for protons and neutrons and additionally the $f_{7/2}$ and $p_{3/2}$ orbits for the neutrons. As is shown in the following discussion, there are many low-lying negative-parity states including $1/2^-$ states. Because there is the possibility for the spin parity of ^{37}Mg ground state to be $1/2^-$ [16], ^{35}Mg may have low-lying $1/2^-$ states and these states could be significantly populated in this experiment. To estimate production cross sections of low-lying $1/2^-$ states in the one neutron knock-out reaction from ^{36}Mg, shell-model calculations in a model space up to the $p_{1/2}$ orbit was also performed, based on the SDPF-M interaction. This effective interaction was made by the combination of USD [42], Kuo-Brown [43], and Millener-Kurath interactions [44,45], which correspond to sd shell,

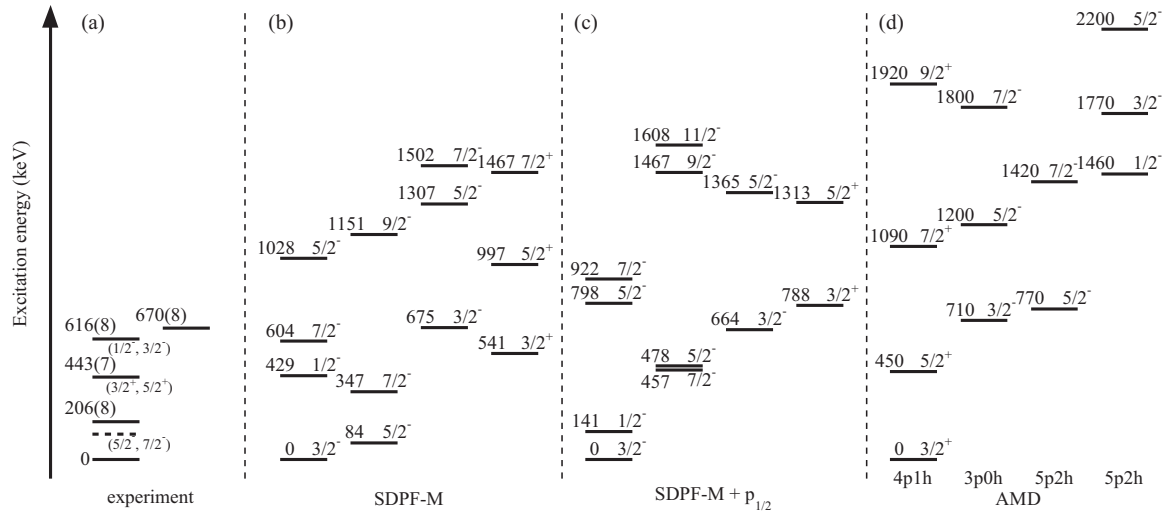

FIG. 4. Experimentally suggested level scheme of ^{35}Mg (a), calculated ones in the shell-model framework with the SDPF-M interaction (b), the SDPF-M interaction including the $p_{1/2}$ orbit (c), and in the AMD framework with the Gogny D1S force (d). In panel (a), spin parity of each state suggested from the analysis of momentum distribution is shown just below the line. An excited state emitting 670(8)-keV γ ray is shown separately because of the difference of γ-ray emission in different reaction channels. Another excited state which is suggested from the analysis of inclusive momentum distribution is shown as dashed line below 200 keV. Excited states up to 1600 or 2200 keV were shown for shell-model or AMD calculations, respectively. In shell-model calculations, excited states connected by large $B(E2)$ values are put together. In the AMD calculation, each band structure is put together and the corresponding particle-hole configuration is shown below. See text for details.

pf shell, and sd-pf cross-shell interactions, respectively. Additional matrix elements related to the neutron $p_{1/2}$ orbit were taken from these interactions. The single-particle energy of the $p_{1/2}$ orbit was calculated to reconstruct the binding energy of ^{41}Ca. With this adjustment, intruder state energies, in ^{32}Mg for instance, become lower than those of the original SDPF-M interaction. Thus, single-particle energies of the pf shell were modified to about 100-keV higher values. Particle-hole excitations were truncated to $4\hbar\omega$ in both calculations. The resulting level schemes of ^{35}Mg are shown in the second and the third from the left in Fig. 4 for without and with the $p_{1/2}$ orbit, respectively. In addition to the level energies, $B(E2)$, $B(M1)$, and $B(E1)$ values as well as spectroscopic factors C^2S of one-neutron knockout reactions from ^{36}Mg were calculated. In this figure, excited states up to 1600 keV connected by large $B(E2)$ values are put together. Theoretical cross sections of $7/2^-$, $3/2^-$, $1/2^-$, $3/2^+$, and $5/2^+$ states were deduced by combining single-particle knockout cross sections calculated by the eikonal reaction theory with the CSC_GM code with the calculated spectroscopic factors from the shell model. Center-of-mass corrections of C^2S, $(A_{\rm proj}/A_{\rm res})^N = (36/35)^N$, where N denotes the principle quantum number of the oscillator shell, were included [46]. An empirical quenching factor $R(\Delta S)$ as discussed in Ref. [47] was not applied because the difference of neutron and proton separation energy of ^{36}Mg is more than 20 MeV and thus $R(\Delta S) \approx 1$. The results are summarized in Tables II and III. It is evident that the theoretical cross sections are larger than experimental values, especially the $\sigma_{\rm th}$ values for the $7/2^-_1$ state at $E_{\rm ex} = 349$ or 457 keV are 54.7 or 46.8 mb for the calculations without or with $p_{1/2}$ orbit, respectively, which are already larger than the inclusive cross section of 37(3) mb measured in this work. In previous one-neutron knockout studies on carbon targets in the island of inversion region performed at similar energies, inclusive cross sections of 74(2), 62(2), and 80(4) mb were obtained for knockout from ^{29,30}Ne and ^{37}Mg, respectively [16,34,48]. These values are much larger than in the present work. Together with the large two-neutron removal cross section of 135(12) mb observed here, it is probable that a large fraction of the experimental spectroscopic strength for the $f_{7/2}$ orbit is beyond the one-neutron separation energy of ^{35}Mg, thus detected as ^{34}Mg in the ZDS. This finding of a high-lying $7/2^-$ state bearing most of the spectroscopic strength is in line with earlier observations in neutron-rich Ne isotopes [34,49].

TABLE II. Excitation energies, spin parities (J^π), and C^2S values calculated with the SDPF-M interaction. Single-particle knockout cross sections $\sigma_{\rm sp}$ for corresponding states are also shown. Theoretical cross sections $\sigma_{\rm th}$ are deduced from $\sigma_{\rm sp}$ and C^2S. See text for details.

$E_{\rm ex}$ (MeV)	J^π	$\sigma_{\rm sp}$ (mb)	C^2S	$\sigma_{\rm th}$ (mb)
0	$3/2^-$	33.3	0.64	23.1
84	$5/2^-$			
347	$7/2^-$	16.5	3.0	54.7
429	$1/2^-$			
541	$3/2^+$	15.2	0.89	14.3
604	$7/2^-$	17.2	0.0035	0.0655
675	$3/2^-$	29.3	0.57	18.1
997	$5/2^+$	16.5	0.034	0.601
1028	$5/2^-$			
1151	$9/2^-$			
1307	$5/2^-$			
1467	$7/2^+$			
1502	$7/2^-$	15.2	0.60	9.92

TABLE III. Same as Table II, but for the calculation with $p_{1/2}$ orbit.

E_{ex} (MeV)	J^π	σ_{sp} (mb)	C^2S	σ_{th} (mb)
0	$3/2^-$	33.3	0.53	19.2
141	$1/2^-$	31.3	0.18	6.17
457	$7/2^-$	16.9	2.5	46.8
478	$5/2^-$			
664	$3/2^-$	30.3	0.82	27.1
788	$3/2^+$	14.2	0.79	11.9
798	$5/2^-$			
922	$7/2^-$	15.8	0.49	8.43
1313	$5/2^+$	16.7	0.032	0.571
1365	$5/2^-$			
1467	$9/2^-$			
1608	$11/2^-$			

TABLE IV. Same as Table II, but for the AMD calculations.

E_{ex} (MeV)	J^π	σ_{sp} (mb)	C^2S	σ_{th} (mb)
0	$3/2^+$	16.1	1.9	32.9
450	$5/2^+$	18.3	0.35	6.78
710	$3/2^-$	30.7	0.42	14.0
770	$5/2^-$	12.2	0.00	0.00
1090	$7/2^+$			
1200	$5/2^-$	11.2	0.01	0.122
1420	$7/2^-$	15.6	0.63	10.7
1460	$1/2^-$	26.4	0.01	0.287
1770	$3/2^-$	27.4	0.01	0.298
1800	$7/2^-$	15.3	0.01	0.167
1920	$9/2^+$			
2200	$5/2^-$	10.6	0.00	0.00

From the analysis of the momentum distribution and the experimental exclusive cross sections, the $3/2^-$ state at 676 keV and the $3/2^+$ state at 554 keV in the shell-model calculation without $p_{1/2}$ orbit are suggested to correspond to the 443(7)- and 616(8)-keV transitions populated in this experiment. The shell model predicts that these two excited states decay to both the ground and first excited $5/2^-$ states. The calculated branching ratio for the decay from the first excited $3/2^-$ to the $3/2^-$ ground state is about 65% and it stays almost the same value when a possible $5/2^-$ state goes to a higher energy of around 200 keV. For this branching ratio estimation, experimental level energies and theoretical $B(E2)$, $B(M1)$, and $B(E1)$ were taken into account. Similarly, the branching ratio of the decay from the first $3/2^+$ state to ground state varies from 66 to 86% if the excitation energy of the $5/2^-$ state changes from 84 to 200 keV. On the contrary, the first $7/2^-$ state at 347 keV decays only to the first $5/2^-$ state when excited energies of these two states are varied.

When the $p_{1/2}$ orbit is added into the model space of the shell-model calculations, the predicted level structure of ^{35}Mg drastically changes. As is shown in Fig. 4, there are possible band structures by comparing $B(E2)$ values. In both calculations with and without $p_{1/2}$ orbit, the band including the ground state can be explained as a $K = 1/2^-$ band whose level ordering is changed due to the decoupling parameter. The second band from the left in Fig. 4 for both shell-model calculations might be a $K = 5/2^-$ band. In the calculations including the $p_{1/2}$ orbit, the excitation energies of the $5/2^-$ and $7/2^-$ states in this $K = 5/2^-$ band change compared to those without $p_{1/2}$ orbit. It may be because of the mixing of the $5/2^-$ states in the $K = 1/2^-$ and possible $K = 5/2^-$ band and that of $7/2^-$ states in these bands, resulting in relatively strong $B(E2)$ values between these states. So the possible explanation of the drastic change between the two shell-model calculations is this mixing and the lowering of the first $1/2^-$ state due to adding the $p_{1/2}$ orbit in the model space. Applying the same comparison as discussed above, the 443(7)- and 616(8)-keV γ rays can be assigned to the decay from the $3/2^+$ state calculated at 788 keV to the ground state and from the $3/2^-$ state at 664 keV to the $1/2^-$ state at 141 keV. The latter matches the observed 206(8)-keV γ-ray transition in energy but not in the much lower intensity, thus excluding an assignment of $1/2^-$ to the observed transition at 206(8) keV. Further, the origin of the 670(8)-keV γ ray remains vague.

Also, antisymmetrized molecular dynamics (AMD) calculations were performed with the Gogny D1S force [50], which have been successfully applied to neutron-rich even Ne and Mg isotopes [51]. The results are summarized on the right-hand side of Fig. 4 and in Table IV. Note that the main configuration of ground and first excited states is $4p$-$1h$, which means there is a single hole in the neutron sd shell. They are part of a rotational band, which continues with a $7/2^+$ state at 1090 keV. The $3/2^-$ level at 710 keV and the $5/2^-$ level at 770 keV have different neutron particle-hole configurations of $3p$-$0h$ and $5p$-$2h$, respectively. ^{36}Mg has a neutron $4p$-$0h$ configuration in the AMD calculation resulting in a small C^2S of $5/2^-$ state.

Most striking is the different ground-state spin parities produced by the AMD and shell-model calculations. Contrary to the $3/2^-$ and close-lying $5/2^-$ or $1/2^-$ proposed by the shell model, AMD suggests a spin parity of $3/2^+$ for the ground state of ^{35}Mg. Though there are differences between J^π assignments of the ground and excited states by the observed momentum distribution in this work and the AMD calculation, it is likely that the relative energy difference of different bands varies or is inverted when different model or interactions are used.

By comparing experimental results and theoretical decay scheme in the AMD framework, the 443(7)- and 616(8)-keV γ rays can be assigned to decays from the first $5/2^+$ and from the first $3/2^-$ state to the ground state, respectively, but it is not possible to place the 206(8)- and 670(8)-keV γ rays in this theoretical prediction. Suppose the $3p$-$0h$ band goes down and the $3/2^-$ bandhead becomes the ground state as in the shell model, $1/2^-$ or $3/2^-$ excited states produced by one-neutron knockout from $l = 1$ orbit are more than 1.46 MeV. Also $7/2^-$ states are at 1.42 and 1.80 MeV and they emit 1.07- and 0.60-MeV γ rays decaying to the first $5/2^+$ and second $5/2^-$ states, respectively. Our experimental setup would have been sensitive to these γ-ray energies but they were not observed. It is noted, however, that the trend of production cross sections

for ground and excited states has a better agreement with the experimental results than the shell-model calculations.

Considering the Nilsson diagram, the deformation of ^{35}Mg is strongly related to its ground-state spin and parity. The last neutron in ^{35}Mg occupies the $[202]3/2^+$ orbit when the deformation parameter is $0.3 \leqslant \beta \leqslant 0.5$, but its orbit changes to $[321]1/2^-$ for $0.5 \geqslant \beta$ [52]. The deformation of ^{35}Mg is unknown, but deformation parameters of the neighboring isotopes ^{34,36}Mg of $\beta \sim 0.5$ have been deduced using (p, p') and intermediate-energy Coulomb excitation [17,18,53]. These large deformations and their systematics are well reproduced by the shell-model calculations using different interactions [20,41], as shown in Fig. 5 of Ref. [18]. Combining the experimental results that show there is significant component of the neutron knockout from $l = 1$ or 3 in the inclusive momentum distribution and the theoretical calculations, a spin parity of $3/2^-$ or $1/2^-$ for the ground state of ^{35}Mg, which is highly affected by the decoupling parameter, is indeed likely. At $3/2^-$ it may be the same as for ^{37}Mg, for which $J^\pi = 1/2^-$ could not fully be excluded [16].

V. SUMMARY

The structure of ^{35}Mg was investigated via the one-neutron knockout and two-nucleon removal reactions from ^{36}Mg and ^{37}Al, respectively. Energies and exclusive cross sections of de-excitation γ rays and parallel momentum distributions were measured in coincidence with ^{35}Mg residues. Three observed γ-ray transition energies were consistent with a previous experiment using a different reaction channel, while a new low-lying transition at 206(8) keV was reported. The relative intensities in different reaction channels suggested that the 670(8)-keV γ ray does not originate from the same level as the 616(8)-keV transition. The combined information with momentum distribution revealed that there were significant components of $1n$ knockout from not only the $l = 3$ but also the $l = 1$ orbit and excited states populated by neutron knockout from $l = 3$ were close to the ground state or emitted low-energy γ rays. Furthermore, the low inclusive cross section indicated that a major part of the spectroscopic strength goes beyond the low neutron separation energy of ^{35}Mg. Obtained experimental intensities were compared to shell-model calculations as well as AMD calculations folded with calculated single-particle cross sections. A possible explanation for the disagreement, particularly the much lower inclusive cross section, is based upon the speculation that the $f_{7/2}$ orbit lies much higher in energy than assumed in the shell-model calculations. Further experimental studies of ^{35}Mg need to aim for a higher sensitivity at very low excitation energies and unbound states to clarify the location of the unobserved $f_{7/2}$ strength.

ACKNOWLEDGMENTS

We would like to express our gratitude to the RIKEN Nishina Center accelerator department for providing a stable and high-intensity ^{48}Ca primary beam and thank the BigRIPS team for preparing the secondary beams. S.M. acknowledges the Grant-in-Aid for JSPS Fellows (JP15J08882) from the Ministry of Education, Culture, Sports, Science, and Technology (MEXT), Japan.

[1] E. K. Warburton, J. A. Becker, and B. A. Brown, Phys. Rev. C **41**, 1147 (1990).
[2] X. Campi, H. Flocard, A. K. Kerman, and S. Koonin, Nucl. Phys. A **251**, 193 (1975).
[3] D. Guillemaud-Mueller, C. Détraz, M. Langevin, F. Naulin, M. de Saint-Simon, C. Thibault, F. Touchard, and M. Epherre, Nucl. Phys. A **426**, 37 (1984).
[4] C. Détraz, D. Guillemaud, G. Huber, R. Klapisch, M. Langevin, F. Naulin, C. Thibault, L. C. Carraz, and F. Touchard, Phys. Rev. C **19**, 164 (1979).
[5] T. Motobayashi, Y. Ikeda, K. Ieki, M. Inoue, N. Iwasa, T. Kikuchi, M. Kurosawa, S. Moriya, S. Ogawa, H. Murakami *et al.*, Phys. Lett. B **346**, 9 (1995).
[6] H. Iwasaki, T. Motobayashi, H. Sakurai, K. Yoneda, T. Gomi, N. Aoi, N. Fukuda, Zs. Fülöp, U. Futakami, Z. Gacsi *et al.*, Phys. Lett. B **522**, 227 (2001).
[7] K. Yoneda, H. Sakurai, T. Gomi, T. Motobayashi, N. Aoi, N. Fukuda, U. Futakami, Z. Gacsi, Y. Higurashi, N. Imai *et al.*, Phys. Lett. B **499**, 233 (2001).
[8] J. A. Church, C. M. Campbell, D.-C. Dinca, J. Enders, A. Gade, T. Glasmacher, Z. Hu, R. V. F. Janssens, W. F. Mueller, H. Olliver *et al.*, Phys. Rev. C **72**, 054320 (2005).
[9] P. Doornenbal, H. Scheit, N. Aoi, S. Takeuchi, K. Li, E. Takeshita, H. Wang, H. Baba, S. Deguchi, N. Fukuda *et al.*, Phys. Rev. Lett. **103**, 032501 (2009).
[10] A. Poves and J. Retamosa, Phys. Lett. B **184**, 311 (1987).
[11] J. R. Terry, B. A. Brown, C. M. Campbell, J. M. Cook, A. D. Davies, D.-C. Dinca, A. Gade, T. Glasmacher, P. G. Hansen, B. M. Sherrill *et al.*, Phys. Rev. C **77**, 014316 (2008).
[12] B. Bastin, S. Grévy, D. Sohler, O. Sorlin, Zs. Dombrádi, N. L. Achouri, J. C. Angélique, F. Azaiez, D. Baiborodin, R. Borcea *et al.*, Phys. Rev. Lett. **99**, 022503 (2007).
[13] S. Takeuchi, M. Matsushita, N. Aoi, P. Doornenbal, K. Li, T. Motobayashi, H. Scheit, D. Steppenbeck, H. Wang, H. Baba *et al.*, Phys. Rev. Lett. **109**, 182501 (2012).
[14] L. Gaudefroy, O. Sorlin, D. Beaumel, Y. Blumenfeld, Z. Dombrádi, S. Fortier, S. Franchoo, M. Gélin, S. Grévy, F. Hammache *et al.*, Phys. Rev. Lett. **97**, 092501 (2006).
[15] A. Gade, P. Adrich, D. Bazin, M. D. Bowen, B. A. Brown, C. M. Campbell, J. M. Cook, S. Ettenauer, T. Glasmacher, K. W. Kemper *et al.*, Phys. Rev. Lett. **99**, 072502 (2007).
[16] N. Kobayashi, T. Nakamura, Y. Kondo, J. A. Tostevin, Y. Utsuno, N. Aoi, H. Baba, R. Barthelemy, M. A. Famiano, N. Fukuda *et al.*, Phys. Rev. Lett. **112**, 242501 (2014).
[17] S. Michimasa, Y. Yanagisawa, K. Inafuku, N. Aoi, Z. Elekes, Zs. Fülöp, Y. Ichikawa, N. Iwasa, K. Kurita, M. Kurosawa *et al.*, Phys. Rev. C **89**, 054307 (2014).
[18] P. Doornenbal, H. Scheit, S. Takeuchi, N. Aoi, K. Li, M. Matsushita, D. Steppenbeck, H. Wang, H. Baba, E. Ideguchi *et al.*, Phys. Rev. C **93**, 044306 (2016).
[19] P. Doornenbal, H. Scheit, S. Takeuchi, N. Aoi, K. Li, M. Matsushita, D. Steppenbeck, H. Wang, H. Baba, H. Crawford *et al.*, Phys. Rev. Lett. **111**, 212502 (2013).

[20] E. Caurier, F. Nowacki, and A. Poves, Phys. Rev. C **90**, 014302 (2014).
[21] J. A. Tostevin, Nucl. Phys. A **682**, 320 (2001).
[22] B. A. Brown, P. G. Hansen, B. M. Sherrill, and J. A. Tostevin, Phys. Rev. C **65**, 061601(R) (2002).
[23] P. G. Hansen, Phys. Rev. Lett. **77**, 1016 (1996).
[24] P. G. Hansen and B. M. Sherrill, Nucl. Phys. A **693**, 133 (2001).
[25] B. Abu-Ibrahim, Y. Ogawa, Y. Suzuki, and I. Tanihata, Comput. Phys. Commun. **151**, 369 (2003).
[26] A. Gade, D. Bazin, B. A. Brown, C. M. Campbell, J. M. Cook, S. Ettenauer, T. Glasmacher, K. W. Kemper, S. McDaniel, A. Obertelli *et al.*, Phys. Rev. C **83**, 044305 (2011).
[27] T. Kubo, D. Kameda, H. Suzuki, N. Fukuda, H. Takeda, Y. Yanagisawa, M. Ohtake, K. Kusaka, K. Yoshida, N. Inabe *et al.*, Prog. Theor. Exp. Phys. **2012**, 03C003 (2012).
[28] N. Fukuda, T. Kubo, T. Ohnishi, N. Inabe, H. Takeda, D. Kameda, and H. Suzuki, Nucl. Instrum. Methods Phys. Res., Sect. B **317**, 323 (2013).
[29] K. Kimura, T. Izumikawa, R. Koyama, T. Ohnishi, T. Ohtsubo, A. Ozawa, W. Shinozaki, T. Suzuki, M. Takahashi, I. Tanihata *et al.*, Nucl. Instrum. Methods Phys. Res., Sect. A **538**, 608 (2005).
[30] H. Kumagai, A. Ozawa, N. Fukuda, K. Sümmerer, and I. Tanihata, Nucl. Instrum. Methods Phys. Res., Sect. A **470**, 562 (2001).
[31] S. Takeuchi, T. Motobayashi, Y. Togano, M. Matsushita, N. Aoi, K. Demichi, H. Hasegawa, and H. Murakami, Nucl. Instrum. Methods Phys. Res., Sect. A **763**, 596 (2014).
[32] P. Doornenbal, Prog. Theor. Exp. Phys. **2012**, 03C004 (2012).
[33] S. Agostinelli, J. Allison, K. Amako, J. Apostolakis, H. Araujo, P. Arce, M. Asai, D. Axen, S. Banerjee, G. Barrand *et al.*, Nucl. Instrum. Methods Phys. Res., Sect. A **506**, 250 (2003).
[34] H. N. Liu, J. Lee, P. Doornenbal, H. Scheit, S. Takeuchi, N. Aoi, K. A. Li, M. Matsushita, D. Steppenbeck, H. Wang *et al.*, Phys. Lett. B **767**, 58 (2017).
[35] ATIMA code, http://web-docs.gsi.de/∼weick/atima/.
[36] P. Doornenbal, P. Reiter, H. Grawe, T. Saito, A. Al-Khatib, A. Banu, T. Beck, F. Becker, P. Bednarczyk, G. Benzoni *et al.*, Nucl. Instrum. Methods Phys. Res., Sect. A **613**, 218 (2010).
[37] M. Wang, G. Audi, A. H. Wapstra, F. G. Kondev, M. MacCormick, X. Xu, and B. Pfeiffer, Chin. Phys. C **36**, 1603 (2012).
[38] O. Tarasov and D. Bazin, Nucl. Instr. Meth. B **266**, 4657 (2008).
[39] H. Olliver, T. Glasmacher, and A. E. Stuchbery, Phys. Rev. C **68**, 044312 (2003).
[40] N. Shimizu, arXiv:1310.5431 [nucl-th].
[41] Y. Utsuno, T. Otsuka, T. Mizusaki, and M. Honma, Phys. Rev. C **60**, 054315 (1999).
[42] B. A. Brown and B. H. Wildenthal, Annu. Rev. Nucl. Part. Sci. **38**, 29 (1988).
[43] T. T. S. Kuo and G. E. Brown, Nucl. Phys. A **114**, 241 (1968).
[44] E. K. Warburton, D. E. Alburger, J. A. Becker, B. A. Brown, and S. Raman, Phys. Rev. C **34**, 1031 (1986).
[45] D. J. Millener and D. Kurath, Nucl. Phys. A **255**, 315 (1975).
[46] P. G. Hansen and J. A. Tostevin, Annu. Rev. Nucl. Part. Sci. **53**, 219 (2003).
[47] J. A. Tostevin and A. Gade, Phys. Rev. C **90**, 057602 (2014).
[48] N. Kobayashi, T. Nakamura, Y. Kondo, J. A. Tostevin, N. Aoi, H. Baba, R. Barthelemy, M. A. Famiano, N. Fukuda, N. Inabe *et al.*, Phys. Rev. C **93**, 014613 (2016).
[49] S. M. Brown, W. N. Catford, J. S. Thomas, B. Fernández-Domínguez, N. A. Orr, M. Labiche, M. Rejmund, N. L. Achouri, H. Al Falou, N. I. Ashwood *et al.*, Phys. Rev. C **85**, 011302(R) (2012).
[50] J. Dechargé and D. Gogny, Phys. Rev. C **21**, 1568 (1980).
[51] M. Kimura, T. Suhara, and Y. Kaneda-En'yo, Eur. Phys. J. A **52**, 373 (2016).
[52] S. Watanabe, K. Minomo, M. Shimada, S. Tagami, M. Kimura, M. Takechi, M. Fukuda, D. Nishimura, T. Suzuki, T. Matsumoto *et al.*, Phys. Rev. C **89**, 044610 (2014).
[53] H. Iwasaki, T. Motobayashi, H. Sakurai, K. Yoneda, T. Gomi, N. Aoi, N. Fukuda, Zs. Fülöp, U. Futakami, Z. Gacsi *et al.*, Phys. Lett. B **620**, 118 (2005).